Planar granular shear flow under external vibration

Eric P. Hoppmann and Brian C. Utter

Phys. Rev. E **96**, 022903 — Published 16 August 2017

DOI: 10.1103/PhysRevE.96.022903

Planar granular shear flow under external vibration

Eric P. Hoppmann[1] and Brian C. Utter[1,2*]
[1] *Department of Physics and Astronomy, James Madison University, Harrisonburg, VA 22807 and*
[2] *Department of Physics and Astronomy, Bucknell University, Lewisburg, PA 17837*
(Dated: July 31, 2017)

We present results from a planar shear experiment in which a two dimensional horizontal granular assembly of pentagonal particles sheared between two parallel walls is subjected to external vibration. Particle tracking and photoelastic measurements are used to quantify both grain scale motion and interparticle stresses with and without imposed vibrations. We characterize the particle motion in planar shear and find that flow of these strongly interlocking particles consists of transient vortex motion with a mean flow given by the sum of exponential profiles imposed by the shearing walls. Vibration is applied either through the shearing surface or as bulk vertical vibration of the entire shearing region with dimensionless accelerations $\Gamma = A(2\pi f)^2/g \approx 0-2$. In both cases, increasing amplitude of vibration A at fixed frequency f leads to failure of the force network, reduction in mean stress, and a corresponding reduction in imposed strain. Vibration of the shearing surface is shown to induce the preferential slipping of large angle force chains. These effects are insensitive to changes in frequency in the range studied ($f = 30-120$ Hz), as sufficiently large displacements are required to relieve the geometrical frustration of the jammed states.

I. INTRODUCTION

The flow of dense granular materials is frequently marked by shear banding, the coexistence of seemingly solid- and fluid-like regions, and large stress and velocity fluctuations in both space and time. One fruitful approach to understanding failure in these systems is through the jamming/unjamming transition [1–3] in which the system is driven, for instance by shear or vibration, through an energetic barrier arising from geometrical frustration. The jamming picture has been applied to many systems in which motion is impeded due to geometrical constraints, from foams and emulsions to traffic flows. In this picture, key factors in the formation and breaking of isotropic jammed states include particle density, shear, and granular temperature, or velocity fluctuations. Shear can additionally lead to jamming of systems close to the isotropic jamming point by inducing anisotropies in the stress network [3].

Under shear, granular systems commonly transition between metastable states which contain system spanning force chains which resist the shear. While these force chains are strong in the compressive direction, forming a structural backbone for the granular assembly, they can be fragile in the transverse direction, in which a small lateral force may be sufficient to cause buckling of chains [3, 4]. In practice, a background pressure of weak lateral forces can be sufficient to stabilize the strong force network. Consequently, the stability of a jammed, sheared system may depend on properties of the weak force network and confining pressure as well as the nature of the shear and vibration protocols.

Vibration leads to such phenomena as triggering of avalanches and protocols to prevent jamming in industrial transport applications. An important example of a system which becomes clogged and unjammed due to vibration is hopper flow, of both scientific and practical significance. Specifically, arch formations at the orifice occur at the same probibilistic rate with and without vibration but are found to be destabilized due to vibration [5, 6]. For these systems, the relevant parameter determining mean flux through the orifice is the maximum velocity of the vibrating motion [7, 8]. In vibrated beds of particles, jamming behaviors are typically history dependent [9] with the nonlinear response of the system dominated by contact-breaking due to the purely repulsive interaction between grains [10]. Under shear, the stress in both vibrated and non-vibrated granular materials is non-monotonic as a function of strain rate, with vibration reducing static shear strength, while still exhibiting history dependence for relatively high vibrations [11]. Shear and vibration were also found to produce an order/disorder transition in monodisperse granular materials in an annular geometry [12].

We report on experiments using a planar shear geometry, in which the granular material is sheared between two boundaries moving in opposite directions. An advantage of this geometry, commonly used in simulations with periodic boundary conditions [13, 14], is that uniform shear across the channel can be imposed in the absence of gravity or curved shearing surfaces. Planar shear simulations typically exhibit an approximately linear velocity profile with correlated motion [14]. A linear profile is predicted for inelastic frictionless spheres when the granular temperature and density profile across the channel are uniform [15]. Experimentally, this geometry is rarely employed since, in the absence of periodic boundary conditions, grains must recirculate at the ends of a channel and the central region approximates planar shear with, on average, a constant particle density. Couette and simple shear geometries are more commonly used experimentally. In these systems, dilation at the shear-

*Electronic address: brian.utter@bucknell.edu

ing surface, shear bands of ≈10 grain diameter widths, and exponentially decaying velocity profiles across the shear band are typically observed. The planar shear geometry has been used in experiments by Miller *et al.*[16], who observe eddies and deviations from a linear velocity profile, for which they develop an analytical model that accurately captures the velocity profile in their system of sheared disks. In the results presented below, we find a different functional form based on exponential velocity profiles driven by the two shearing boundaries.

Transient vortex or eddy flow has been observed in a number of sheared systems; we have observed vortices and exponential velocity profiles in the Couette geometry [17], but a number of other examples include those in simple shear [18, 19], in which a rectangular array of particles is deformed smoothly into a parallelogram, biaxial or triaxial strain [20, 21], and a similar plane strain compression [22]. In cases for which shear banding occurs, vortices are dominant flow features within the shear band [21, 22]. We choose a channel width comparable to the shear band length; this induces an approximately linear velocity profile in the center of the channel as commonly imposed in simulations, however the flow is essentially a single system-spanning shear band composed of transient vortices.

In this paper, we study a two-dimensional assembly of photoelastic grains to study the stress response of the grains in addition to measuring kinematic properties during planar shear. We add external vibrations, imposed either through a single shearing boundary or through vertical/bulk vibration of the entire system, and characterize the force network and particle flow. We find that increasing the amplitude of vibration, either of the shearing surface or the entire shear region, leads to a dramatic decrease of the force network and mean flow rates, while varying the frequency of vibration at fixed amplitude in contrast has little effect. For vibration of the shearing surface, this occurs due to preferential slipping of large force chains at the shear wall boundary, as evidenced by high speed video and distributions of force chain contact angles.

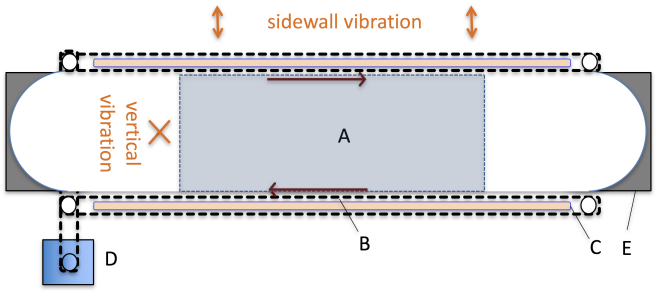

FIG. 1: Experimental schematic (top view). A single layer of photoelastic grains (A) lies horizontally, confined above and below by acrylic plates. Shearing belts (B) held in position by fixed guide rails (C) move in opposite directions to apply shear. The belts move in equal and opposite directions and are driven by a single stepper moter (D). Circular end caps (E) contain the grains at the end of the channel. Vibration can be imposed through one of the shearing walls (sidewall) or vertically by shaking the entire experiment. Grains within the shaded region are imaged for analysis.

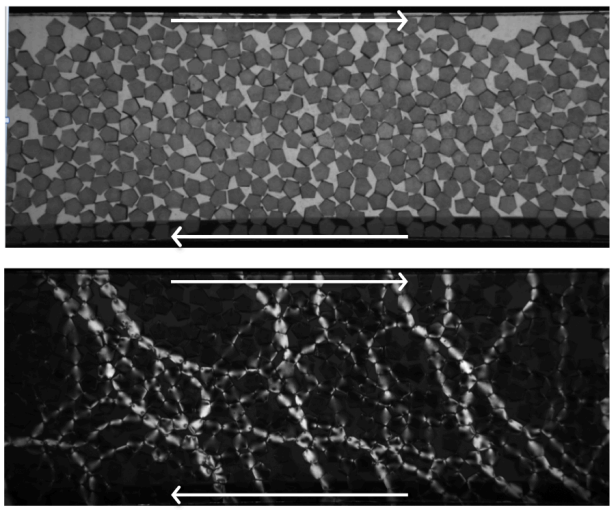

FIG. 2: Experimental images under shear (indicated by arrows) corresponding approximately to the shaded region in Figure 1. (top) Pentagonal grains (unmarked). Grains can also be marked with rectangular tag for automated particle tracking. (bottom) Photoelastic image of force network.

II. EXPERIMENTAL PROCEDURES

The experiment consists of a quasi two-dimensional shearing apparatus as shown in Figure 1. Photoelastic grains lie horizontally in a plane confined between two shearing belts moving at equal speeds in opposite directions to produce a central region of approximately planar shear flow.

The pentagonal grains (mean diameter $d \approx$ 5-7 mm, thickness = 0.30 cm) prevent ordered packing and lead to significant interlocking and correlated motion compared to smooth grains. Grains are composed of a compressible, photoelastic material (Vishay PSM4, elastic modulus = 4 MPa), allowing simultaneous measurement of compression forces and trajectories of the particles [23–25]. Due to photoelasticity, or stress-induced birefringence, grains alter the phase of transmitted light when under stress. By using crossed polarizers, one above and one below the experiment, we can visualize stresses within the grains. Figure 2 shows typical experimental images of the pentagonal grains (top) and photelastic image during shear (bottom). Simple shear can be viewed as compression along one axis (diagonally across the shear region) and dilation along a perpendicular axis with the primary force chains resisting motion of the belts.

The length of the shearing region (37 cm ≈ 60d) is large compared to the width (8.8 cm ≈ 15d), such that the central region approximates planar shear flow in the

field of view of the camera. We confirm through particle tracking that the velocity profile is symmetric and the average cross-channel velocity is zero along the length of the imaging region. By symmetry, the shear flow has zero steady-state mean flow in the image region and the channel is sufficiently narrow to prevent shear banding within the channel. Each end corresponds to a recirculation region in which grains carried in by one belt are recirculated and returned to the central shearing region. The semi-circular end cap prevents significant jamming avoid influencing the region of interest.

Grains are confined vertically between two cast acrylic sheets with a fixed packing fraction of $\phi \approx 0.70$ corresponding to a sample under significant compression. Near the jamming point, intermittency and history dependence is observed as the range of packing fractions supported by a sample of pentagonal grains can either span the shearing gap and support stresses or compact such that no particle motion is observed. A gap is maintained at slightly larger than the grain thickness (≈ 0.35 cm) to ensure grains remain in a nearly 2D plane. A dry lubricant is used between the grains and acrylic base plate. Grains are under significant compression from the sidewalls, with mean stresses significantly larger than the magnitude of the friction force.

Two belts form the channel walls and are driven in opposite directions. Both belts are driven by a single rotary stepper motor to maintain equal belt speeds and zero mean flow in the shearing region. The belt speed is maintained in a slow, quasistatic regime in which the dynamics are a function of the displacement of the shearing surface and results are independent of belt speed. The belts are rough on the grain scale. A typical speed of the shearing surface used in the present study is 0.37 cm/s $\approx 0.5d$/s, corresponding to a mean shear rate of ≈ 0.03. A rigid guiding rail is fixed behind the belt to maintain its position as the stress within the granular material fluctuates.

Vibration of the shearing region is imposed in one of two ways: (i) vibration of the shearing surface, in which one of the driving belts is vibrated perpendicular to the shearing direction by vibrating the guide rail, or (ii) bulk vibration, in which the entire shear channel is vibrated vertically while the side walls are fixed in place. In the present study, the vibration amplitude A and frequency f can be independently varied to determine the peak vibration acceleration, sometimes indicated as a dimensionless acceleration relative to gravitational acceleration [26], $\Gamma = A(2\pi f)^2/g$. In practice, the frequency is imposed, the acceleration is experimentally measured for a chosen amplitude, and the amplitude is defined as $A \equiv \Gamma g/(4\pi^2 f^2)$. Here we use $f = 30 - 120$ Hz and reach accelerations of $\Gamma = 0 - 2$ such that $A = 0 - 0.5$ mm. The frequency is much larger than the shearing rate in all cases.

For (i) vibration of the shearing surface, one of the guide rails is connected to two small electromagnetic shakers powered in parallel by a sinusoidal function generator. The output signal is monitored by an oscilloscope and the acceleration of the rail is measured by an accelerometer. We cannot measure the acceleration of the shearing surface directly, but while the system is compressed, the position of the guide rails sets the location of the shearing belt. With the grains under compression in this mode, the volume fluctuates at most on the order of 0.5%.

To perform (ii) vertical vibration, the entire experiment is cantilevered over a fulcrum and attached to an electromagnetic shaker (VTS-65). This allows us to illuminate the experiment from below to perform photoelastic measurements. An accelerometer is attached to the channel to measure the imposed vertical vibration.

The experiment is illuminated from below and imaged using a camera from above. We acquire images, typically at a rate of 2 Hz in runs of 1000-10,000 images. Images can either be taken without polarizers to measure particle locations or with polarizers in place to measure the internal stresses (Figure 2(bottom)). Mean stress is measured using the gradient squared method [23] in which the mean gradient in image intensity averaged over a region of pixels is found to monotonically increase with local stress. Additionally, particles can be marked with rectangular bars to enable tracking of particle positions and velocities.

III. RESULTS

We impose external vibrations to probe the response of the system as it explores a sequence of jammed configurations.

A. Flow profile

The pentagonal grains used here are strongly interlocking [27], leading to significant cooperative motion. Transient vortices, or eddies, are ubiquitous in this flow as shown in Figure 3, which displays the velocity field during a time corresponding to a strain of approximately 25%. We note that this image is the velocity field itself as opposed to the residual displacement field, in which the mean velocity is subtracted, typically used to image vortex motion. These vortices are short-lived, but generally present throughout the experiment. The central region typically exhibits plug-like flow in which a group of particles (of diameter $\approx 10d$) rotates as a unit before breaking apart and reforming as a subsequent cluster. Such behavior is expected when the timescale of energy dissipation is much faster than the inverse strain rate [28] and is closely related to force chain buckling as a generic structure observed in shear bands [21] and acting as a mechanism to relieve macroscopic stresses in the system given the interlocking of particles [22]. Indeed, as discussed below, diagonal force chains form, rotate past vertical, and fail during this process. Unlike typical fluid

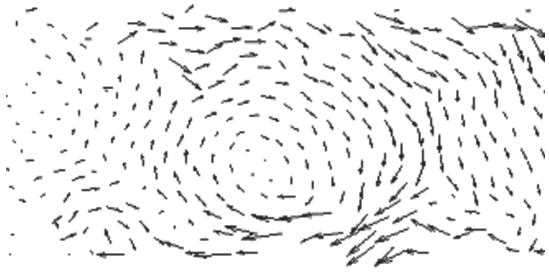

FIG. 3: A commonly-observed transient vortex in the velocity field in which a cluster of grains rotates in a cooperative motion of constituent grains. The total time is 7 seconds corresponding to a displacement of the shearing surface of $\approx 3.5d$.

systems, these are non-inertial vortices in the sense that the momentum and vorticity immediately vanish if the stresses are removed. Rather, the vortices observed are geometric effects as motion of a given grain in a dense interlocking granular flow requires coordinated motion of its neighbors. In this sense, a vortex is a self-contained transient jammed cluster that moves according to the shear imposed by the surrounding medium and interlocking of the pentagonal grains contributes to the stability of these clusters.

The mean velocity profiles versus distance across the channel, averaging over individual vortex events, are however very regular as shown in Fig. 4(a) for different vertical vibrations. The velocity across the channel is clearly not linear, as was also found in the work of Miller *et al.*[16], but we find a different functional form for the mean velocity profile. At each Γ, $v_x(y)$ is well fit by a sum of exponential velocities driven by each shearing surface,

$$v_x(y) = v_0\left(e^{-y/\ell} - e^{-(W-y)/\ell}\right), \qquad (1)$$

where v_0 is the velocity at each shearing surface, W is the width of the channel, and ℓ is the length scale of the exponential. This is confirmed for particles within $\approx 5d$ of the shearing surfaces by plotting on a log-lin scale. An example is shown (solid line, Fig. 4(a)) matching the $\Gamma = 0$ data set (open blue squares) for which $v_0 = 0.45d/\mathrm{s}$ and $\ell = 2.5d$. In Fig. 4(b), we plot the shear rate corresponding to the four lowest vibration amplitudes in Fig. 4(a). The line plotted with the data corresponds to a fit using Eq. 1. This data is in clear contrast to the data in [16], though we note that in the present results, pentagonal, rather than circular, grains are used and the packing fraction frequently decreases near the shearing surface. The central region, from around $3d$ to $12d$, or 60% of the shearing region, can also be reasonably approximated using a linear fit.

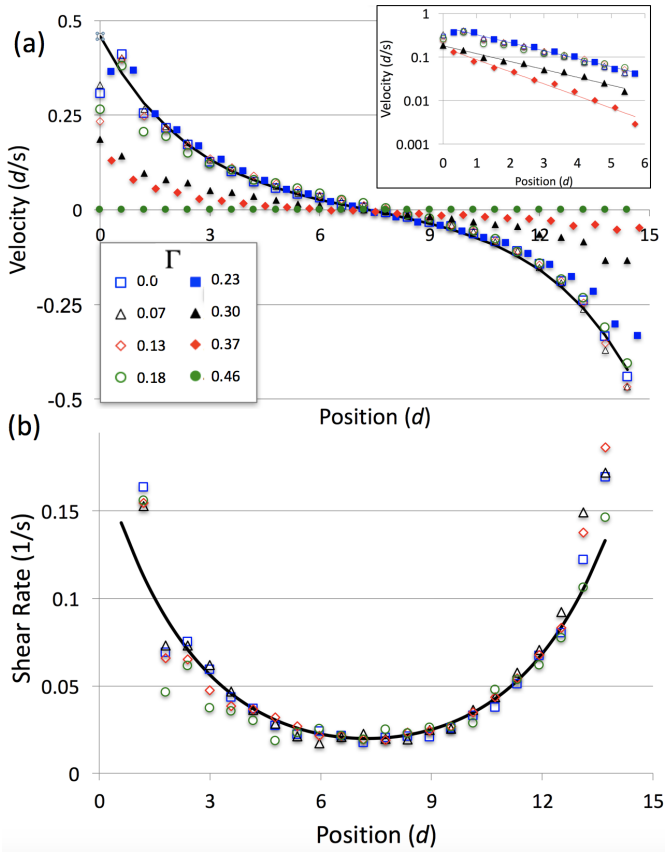

FIG. 4: (a) Mean velocity versus distance across the shearing channel. The overall velocity scale decreases with vibration amplitude with a corresponding decrease in stress. The solid line is a fit to the $\Gamma = 0.23$ data set using a sum of two exponential velocity profiles at the shearing surface (Eq. 1, $v_0 = 0.45d/\mathrm{s}$, $\ell = 2.5d$, and $W = 14.5$). The inset shows a log-lin plot of $v_x(y)$, which is observed to be linear for each data set, confirming the exponential behavior for $y < 0$. $\Gamma = 0.46$ is omitted as $v_x \approx 0$. (b) Shear rate for the four smallest vibrations from (a). The solid line corresponds to dv_x/dy using Eq. 1 and the same parameters from part (a).

B. Stress network with vibration of shearing surface

Particle motion and interparticle forces are inhomogeneous in both space and time. Typically, mean stress in the system fluctuates significantly, as shown in Figure 5, with fluctuations of the same order of magnitude as the mean value, indicated by the horizontal line. Force chains form and break as local configurations become jammed and unjammed, leading to the large fluctuations observed.

In Figure 6, we show the stress versus time for runs with different vibration amplitudes. The data sets are offset vertically for clarity, with plots corresponding to higher vibration displaced lower on the graph. It is apparent that larger vibration amplitude leads to both a reduction in stress and longer quiescent periods between

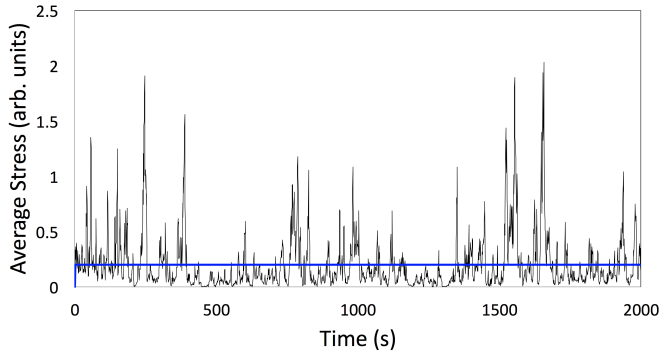

FIG. 5: Mean stress versus time during shear. Strong fluctuations are observed compared to the mean stress (horizontal line).

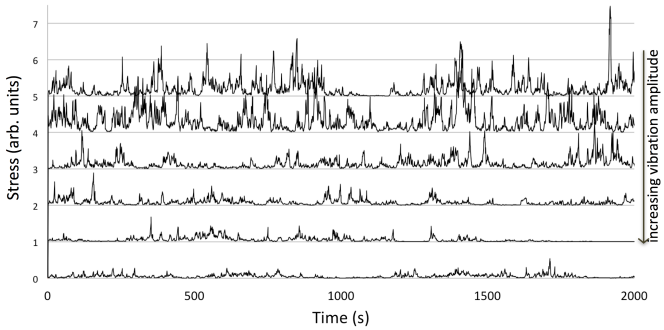

FIG. 6: Stress versus time. Individual runs of mean stress versus time are plotted for varying vibration amplitude at f =30 Hz. Each data set, corresponding to $A \approx 0$, 0.03, 0.1, 0.2, 0.3, and 0.4 mm, is shifted vertically by integer values after the background σ_{bg} is subtracted.

bursts of stress activity. As a result, we find that the standard deviation for a given run increases approximately linearly with the mean value of the stress.

We find that increasing vibration amplitude leads to a sharp decrease in stress within the system, while increasing frequency has little impact in the range of frequencies tested. That is, amplitude rather than Γ or f specifically is the relevant control parameter. This also suggests that the velocity scale Af is not the primary control variable, unlike hopper flow [7, 8]. We show below that vibration induces slipping at the shearing surface, allowing the bulk stress within the system to relax. In Figure 7, we plot the mean stress versus amplitude (at fixed frequency) and versus frequency (at fixed amplitude). The plots span a similar range of Γ (= 0 – 1.6), however, the mean stress is sensitive to the amplitude of vibration rather than frequency, with larger amplitude vibration leading to smaller mean stress.

The amplitude of zero appears to have a lower stress than small amplitude vibration, suggesting that vibration leads to small-scale rearrangements and strengthening of the packing. This is confirmed in Fig. 8 which shows a discrete probability function for stress at various

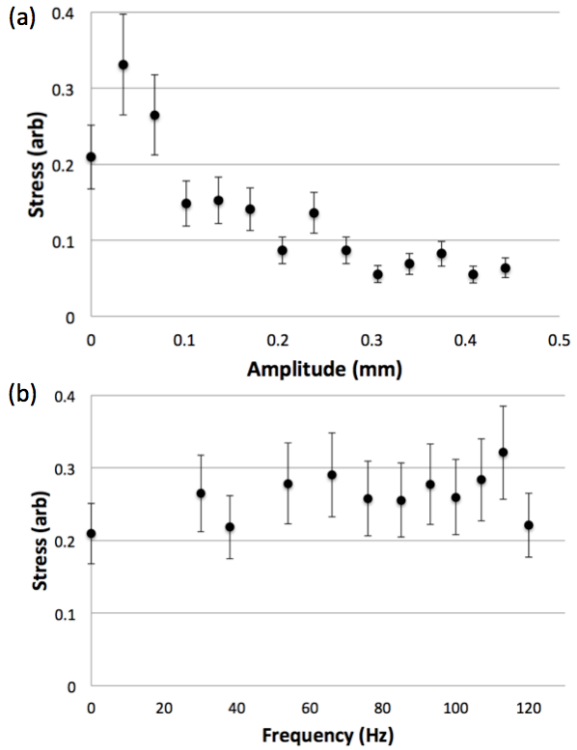

FIG. 7: (a) Stress versus amplitude at fixed frequency (f = 30 Hz). (b) Stress versus frequency at fixed amplitude (A = 0.07 mm). Both data sets correspond to a a similar range of Γ = 0 – 1.6. Error bars indicate the standard deviation for the stress time series which increases with mean stress and is around 20% for most parameter values.

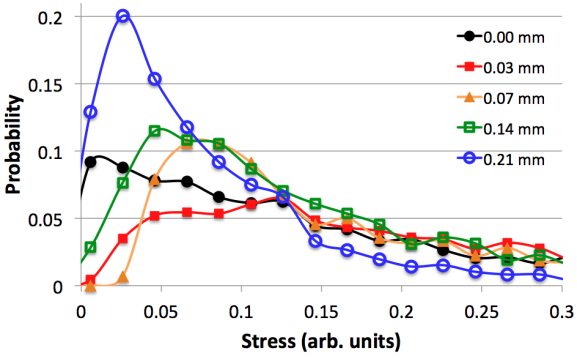

FIG. 8: Discrete probability distribution function for stress at various vibration amplitudes corresponding to the data shown in Fig. 7 (top). Each consists of 2036 data points or 17 minutes of data.

vibration amplitudes corresponding to Fig. 7. We find that a small vibration amplitude actually has a smaller probability for a low stress state compared to the non-vibrated case. Further increasing vibration amplitudes increases the peak near zero stress at the expense of high stress states. Since the walls are rough, high frequency vibration may reduce the effective friction between con-

tacts, while larger displacements are needed to relieve the geometrical frustration of interlocking grains. These observations are consistent with prior measurements of avalanching in a rotating drum which show that amplitude rather than frequency is the relevant control parameter [29] and that small vibrations lead to compaction and strengthening compared to the non-vibrated case [27].

With vibration of the shearing surface, increasing amplitude increases the space available sufficiently to allow relaxation and slipping of force chains. The amplitude at which significant vibration effects are evident though corresponds to a change in volume and packing fraction of only around 0.1% indicating that a small motion of the confining wall supporting the stress allows significant stress relaxation. Given that the mean stress would change only marginally with such a small change in packing fraction, this suggests that it is the motion of the shearing surface itself and corresponding slipping of force chains that lead to the reduction of observed stress. Particles used here are elastic (modulus = 4 MPa) and under compression, so this effect may be more pronounced for rigid grains.

Since stress imposed through the shearing surface drives particle motion, mean stress in the system is also well correlated with the mean velocity of the grains at a fixed distance from the shearing surface. That is, the decrease in stress observed in Fig. 7 corresponds to the decrease in the velocity scale v_0 in Fig. 4.

C. Failure mechanism

Images recorded at higher frame rates reveal that vibration induces slipping at the sidewall as in Figure 9. There, sequential images separated by 0.2 seconds are extracted from a video at 30 Hz near a shearing boundary moving at 0.5 d/s. The horizontal line indicates a fixed position in the lab frame and a grain in contact with the shearing surface moving upwards is indicated by the circle. A slippage event causes the grain to slide backwards relative to the shearing surface and the stress to be relieved. This transition is abrupt, and initiating or ceasing sufficiently large vibration leads to a rapid decrease in the stress network. This is in contrast to the dominant reason for the stress drops and fluctuations themselves (e.g. Fig. 5), which occur as individual strong force chains form at approximately 45°, rotate past vertical, fail and subsequently either form additional force chains or enter a quiescent period based purely on the current packing geometry. In the absence of vibration, slip events are rare and individual grains typically move or rotate without slip when in contact with the shearing surface. Since the grains are soft and under compression, we do not typically observe distinct breaking of interior force chains.

This slipping due to failure preferentially relieves stress carried by large angle force chains. In Fig. 10, we show

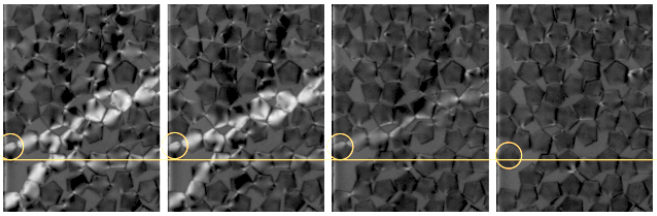

FIG. 9: Sequential images at an interval of 0.2 seconds from an image sequence at 30 Hz showing a typical slip event at the shearing boundary (left edge of images). The boundary grain supporting the stress (circle) slips backwards relative to a fixed position (line) and relieves the stress in the force chain.

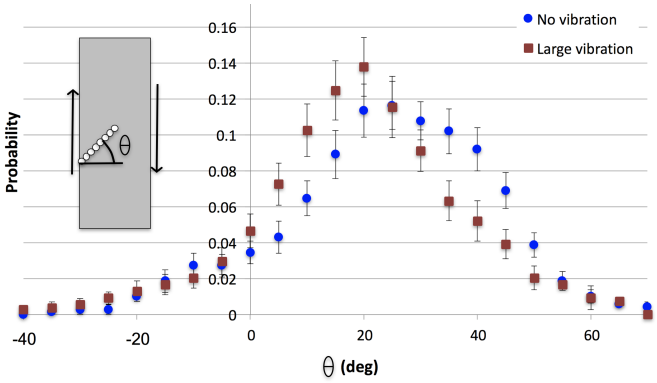

FIG. 10: Distribution of angles for force chains in the absence of vibration (•) and large vibration (▪, $A \approx 0.2$ mm and $f = 30$ Hz).

distributions of the angle at which force chains, composed of chains of particles with forces greater than the mean, contact the shearing surface. The distribution is shifted to smaller angles (from approximately 30° to below 20° in this case) when vibration is turned on.

D. Stress network with bulk vibration

We find that bulk vibration, that is, vertical vibration of the entire shearing region, leads to a qualitatively similar failure of the stress network. As above, we find no significant correlation between average stress and dimensionless acceleration when vibration frequency is the control parameter while an increase in vibration amplitude produces a significant effect, as shown in Fig. 11. In this case, we show plots versus Γ given that one might expect $\Gamma = 1$ to be an upper bound on stability, but failure occurs well below this threshold and with a more gradual drop to zero compared to shearing wall vibration. The failure mechanism appears to differ from forcing at the shearing surface in that sudden relaxation of the entire force network occurs in the absence of a clear signature of slipping at any particular location given the resolution of the data. It may be reasonable that bulk agitation, which

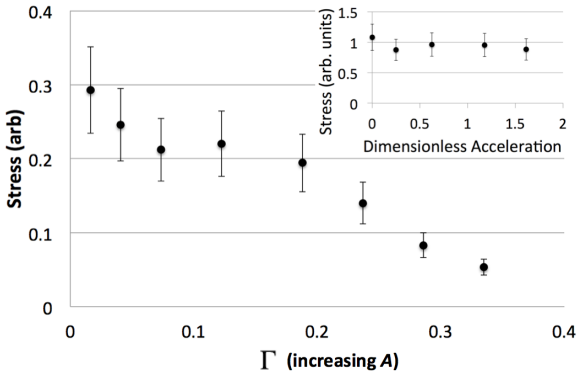

FIG. 11: Average stress versus dimensionless acceleration for bulk vibration at fixed frequency and increasing amplitude. Inset shows stress versus dimensionless acceleration at fixed amplitude and increasing frequency.

impacts all grains rather than only those at the shearing boundary, could be an efficient mechanism for decreasing stress in the system; however, there is no sign of internal force chain breaking, which is perhaps also not surprising for soft particles under compression. The character of the stress drop may well depend on the hardness of the particles used.

IV. DISCUSSION

We find that force networks and particle flow in a two dimensional granular planar shear system are significantly impacted by imposed vibrations.

In the absence of vibration, the mean velocity profile is well described by the sum of two exponentials driven by the shearing surface, with the central region (≈ 20 – 80% of the channel width) reasonably approximated by a linear fit. This is different than the velocity profile measured in work of [16], but the present results differ in that pentagonal, rather than circular, grains are used and a decrease in packing fraction is generally observed close to the shearing surface.

On shorter time scales, flow is dominated by the formation of transient vortices as observed in other shear measurements. This vortex flow is likely even more pronounced given the strongly interlocking pentagonal particles in a geometry that is effectively a shear band, for which vortex flow is a major component [21, 22]. We expect to further probe the flow in the non-vibrated case in future work.

While vibration is typically characterized based on the dimensionless acceleration, we find that increasing the amplitude of vibration has a significant effect while the system is relatively insensitive to changes in vibration frequency. In particular, the scale of the mean stress and velocity diminish with increased vibration amplitude. This is different from measurements of flow rates of hoppers, for which the peak velocity of the vibratory motion is the control parameter. In these cases though, the flow rate to be maximized is driven by a body-force (gravity) and impeded by jamming (arch formation), and imposing vibration decreases the stability of these arches while gravity provides a load that may lead to additional arch formation. In our case, jamming and flow are both driven by the shearing boundary. In the case of forcing from the shearing boundary, the reduction in stress and particle flow occurs due to force chains slipping at the boundary, rather than failure of the force network in the bulk. Under bulk vibration, a sudden overall relaxation of the force network is observed on the time scale of the present data. We note that the particles used are soft, allowing the system to withstand significant elastic deformation where force chains of harder particles may fail. Additional tests of force network failure, as well as simulations in which particle parameters such as stiffness could be easily varied, would help elucidate these effects.

The mean stress versus time exhibits strong fluctuations, well above the mean, but the mean value is correlated to the velocity scale. That is, system spanning force chains, which are the signature of the stress measurement are indicative of strong contact and compressive forces at the shearing boundary, which drive flow. All of these are therefore suppressed concurrently with vibration.

V. ACKNOWLEDGEMENTS

We gratefully acknowledge the support of the Research Corporation (Cottrell College Science Award No. CC7145/7266) and DOD ASSURE Grant # DMR-0353773.

[1] C. S. O'Hern, L. E. Silbert, A. J. Liu, and S. R. Nagel, Phys. Rev. E **68**, 011306 (2003).
[2] M. Van Hecke, Journal of Physics Condensed Matter **22**, 033101 (2010).
[3] D. Bi, J. Zhang, B. Chakraborty, and R. P. Behringer, Nature **480**, 355 (2011).
[4] C. Liu, S. Qicheng, and F. Jin, Powder Technology **288**, 55 (2016).
[5] A. Janda *et al.*, Europhys. Lett. **87**, 24002 (2009).
[6] C. Lozano, G. Lumay, I. Zuriguel, R. C. Hidalgo, and A. Garcimartin, Phys. Rev. Lett. **109**, 068001 (2012).
[7] M. Hunt *et al.*, Phys. Fluids **11**, 68 (1999).
[8] K. Chen *et al.*, Phys. Rev. E **74**, 24002 (2006).
[9] C. R. K. Windows-Yule, A. D. Rosato, N. Rivas, and D. J. Parker, New Journal of Physics **16**, 063016 (2014).
[10] C. F. Schreck, C. S. O'Hern, and M. D. Shattuck, Granular Matter **16**, 209 (2014).
[11] J. A. Dijksman, G. H. Wortel, L. T. H. van Dellen,

O. Dauchot, and M. van Hecke, Phys. Rev. Lett. **107**, 108303 (2011).
[12] K. E. Daniels and R. P. Behringer, J. Stat. Mech. P07018 (2006).
[13] V. Kumaran, J. Fluid Mech. **632**, 109 (2009).
[14] J. Salazar, Granular Matter **16**, 517 (2014).
[15] N. Xu, C. S. O'Hern, and L. Kondic, Phys. Rev. E **72**, 041504 (2005).
[16] T. Miller, P. Rognon, B. Metzger, and I. Einav, Phys. Rev. Lett. **111**, 058002 (2013).
[17] B. Utter and R. P. Behringer, Phys. Rev. E **69**, 031308 (2004).
[18] F. Radjai and S. Roux, Phys. Rev. Lett. **89**, 064302 (2002).
[19] V. Richefeu, G. Combe, and G. Viggiani, Geotechnique Letters **2**, 113 (2012).
[20] J. F. Peters and L. E. Walizer, J. Engineering Mechanics **139**, 1479 (2013).
[21] A. Tordesillas *et al.*, J. Mech. Phys. Solids **90**, 215 (2016).
[22] S. Abedi, A. L. Rechenmacher, and A. D. Orlando, Gran. Matt. **14**, 695 (2012).
[23] D. Howell, R. Behringer, and C. Veje, Chaos **9**, 559 (1999).
[24] T. Majmudar and R. Behringer, Nature **435**, 1079 (2005).
[25] B. Utter, in *Experimental and Computational Techniques in Soft Condensed Matter Physics*, edited by J. Olafsen (Cambridge University Press, Cambridge, 2010), pp. 230–247.
[26] H. K. Pak and R. P. Behringer, Phys. Rev. Lett. **71**, 1832 (1993).
[27] D. L. Amon, T. Niculescu, and B. C. Utter, Phys. Rev. E **88**, 012203 (2013).
[28] D. Ertas and T. C. Halsey, Europhys. Lett. **60**, 931 (2002).
[29] N. C. Swisher and B. C. Utter, Granular Matter **16**, 175 (2014).